Smart Structures and Systems, *Vol. 28, No. 3 (2021) 425-441*
https://doi.org/10.12989/sss.2021.28.3.425

A framework for fast estimation of structural seismic responses using ensemble machine learning model

Chunxiang Li [1a], Hai Li [1b] and Xu Chen*[2]

[1] *School of Mechanism and Engineering Science, Shanghai University, Shanghai 200072, China*
[2] *International Research Institute of Disaster Science, Tohoku University, Sendai 980-8576, Japan*

(*Received December 25, 2020, Revised April 19, 2021, Accepted May 10, 2021*)

Abstract. While recognized as most rigorous procedure leading to 'exact' structural seismic responses, nonlinear time history analysis is usually time consuming and computational demanding, especially when numerous structures remain to be analyzed. This paper proposes a framework to improve the time efficiency in evaluating the structural seismic demands, using ensemble machine learning models based on 'classification-regression' philosophy. Typical tall pier bridges widely located in southwest China are employed as illustrative examples to validate the efficiency and performance of this proposed framework. The results and discussion show that with properly selected input variables, the proposed ensemble model (ORF-ANN herein) performs better in predicting seismic demands than other single learning algorithms (i.e., ANN and ORF), while the time efficiency is improved over 90%. This proposed model could drastically improve the efficiency for determining structural parameters in preliminary design process, and thus reduce the iterations of trail analysis. Additionally, the model constructed from proposed framework is believed especially favored for evaluating the post-earthquake states/resilience of a region and/or highway network, where thousands of structures might be contained, and conducting nonlinear time history analysis for each one would be prohibitively time consuming and delay the rescue operations.

Keywords: ensemble learning; machine learning framework; post-earthquake resilience assessment; tall pier bridges; time efficiency

1. Introduction

Seismic performance of structures is of great concern in civil engineering, since earthquakes are usually the most devastating loadings that structures might experience during lifetime. Nonlinear time history analysis (NLTHA) procedures are usually employed to estimate the seismic performance of target structures in engineering practice. However, while recognized providing most rigorous results, NLTHA is quite time consuming and computational demanding (Chopra and Goel 2002, Chen *et al*. 2018b), especially for preliminary design process and assessing post-earthquake states of numerous structures.

Recently, machine learning (ML) techniques have gained considerable attention in civil engineering, due to its potential capacity in nonlinear mapping modeling. Xie *et al*. (2020) conducted a state-of-the-art review for the application of machine learning techniques in four topic areas of earthquake engineering, and pointed out that machine learning techniques have a great promise to revolutionize the profession of earthquake engineering; moreover, the more efficient machine learning models are worth exploring to solve grand challenges in earthquake engineering. Quite a few literatures (Ferrario *et al*. 2017, Liu and Zhang 2017, Onat and Gul 2018, Duan *et al*. 2019, Mangalathu *et al*. 2019, Mangalathu and Jeon 2019, Pang *et al*. 2021) also explored the feasibility of using ML techniques in assessing structural seismic performance with less computational efforts and satisfying accuracy. The results showed that these techniques, e.g., random forest (RF) and artificial neural network (ANN), could be promising alternatives to NLTHA in estimating structural demands during earthquakes. RF, which is composed of an ensemble of decision trees (DTs), partitions the data into distinct and non-overlapping regions based on the structure of DTs. The aggregated predictions of all the DTs are then utilized as the output of RF, which possesses the advantages of flexibility, intuitive simplicity, and computational efficiency (Breiman 2001). Mangalathu and Jeon (2019) proposed a methodology combining RF and stripe-based approach to generate or update the bridge-specific seismic fragility curves with reduced computational efforts and less expensive re-simulations. Saeidpour *et al*. (2018) also employed RF to assess the responses of bridges subjected to hurricane events and concluded that RF was the most suitable compared with other ML techniques considered in that paper for predicting hurricane-caused failure. These aforementioned literatures demonstrated the feasibility and efficiency of RF in estimating damage states of civil engineering structures. However, errors might occur due to the fact that the final prediction of RF is the average of

*Corresponding author, Ph.D.,
JSPS International Researach Fellow,
E-mail: xuchen_shu@163.com
[a] Ph.D., Professor, E-mail: Li-chunxiang@vip.sina.com
[b] M.S. Student, E-mail: sea1872@shu.edu.cn

ISSN: 1738-1584 (Print), 1738-1991 (Online)

individual predictions (regression tasks) or the most common class (classification tasks). Moreover, for the typical RF employed in civil engineering, only a single feature is generally considered in the partitioning criteria, which has significant limitations in growing trees, especially for those complicated tasks (Murthy *et al*. 1996, Zhang and Suganthan 2015b).

On the other hand, ANN is another popular ML technique that is usually adopted in predicting structural seismic demands, in which the nonlinear regression function between input variables and outputs are established using neurons (Basheer and Hajmeer 2000). Wang *et al*. (2018b) estimated seismic performance of nuclear power plant equipment with ANN, which led to improved computational efficiency. Liu and Zhang (2017) developed the seismic fragility curves for a steel building using both ANN and finite element (FE) model; the authors concluded that ANN model could produce fragility curves of satisfying accuracy with significantly reduced computational time compared with FE model. These studies showed great potential of applying ANN in predicting seismic behavior of civil engineering structures. However, the performance of this regression method could be deteriorated when imbalanced dataset (i.e., certain subsets among the dataset is smaller (larger) than others) was employed for training (Das and Sengur 2010, Chen *et al*. 2013). In engineer practice, the dataset of training ANN model might always be imbalanced, due to the scarcity of earthquake records for certain sites. Therefore, the seismic performance of structures might not be efficiently predicted using traditional ANN, especially when subjected to excitations with high intensity and leading to damage for structures.

This paper proposes a framework to rapidly estimate the structural seismic responses employing novel ensemble ML model based on 'classification-regression' philosophy. In this model, the original database is first classified into subsets according to the characteristics of data, and then regression models are trained and developed for each subset, which is believed able to perform better than traditional single learning algorithms. To validate the efficacy of this proposed framework and ensemble ML model, they are applied on illustration examples of typical tall pier bridges located in southwest China, considering two types of excitations, namely filtered white noises (FWNs) and artificial seismic motions (ASMs). The efficiency is assessed through comparing the results with those obtained from NLTHA and typical single learning algorithms.

2. Proposed ensemble machine learning model

To overcome the potential drawbacks and improve the stability of single machine learners when applied in civil engineering, this paper proposes and utilizes an ensemble ML model to predict seismic responses of structures. This model is developed based on the 'classification-regression' philosophy, which has been proposed and applied in fields as medicine and biology (Alam *et al*. 2020, Wang *et al*. 2020) and employs single ML techniques to complete the 'classification' and 'regression' tasks. When the raw data from field measuring, experiments and/or reliable numerical analysis are first classified into subsets with similar characters, the regression models are believed able to possess better performance in prediction tasks.

For illustration purpose, the oblique random forest (ORF) and ANN algorithms are employed as base learners to accomplish classification and regression tasks, respectively, in current research. Therefore, these two techniques are briefly introduced in this section, followed by the detailed elaboration of the proposed ensemble model (termed as ORF-ANN model hereafter).

2.1 Oblique random forest (ORF)

ORF is a non-parametric algorithm composed of an ensemble of oblique decision trees (ODTs), and developed based on two strategies termed as bootstrap sampling and randomly feature selection. Researchers have demonstrated that the ORF could be more efficient than traditional random forest (RF) in diverse domains (Zhang and Suganthan 2015a, 2017), due to the oblique splits adopted in its structure (Murthy *et al*. 1996). Among the ORF, each ODT construction could provide prediction results by classifying the original dataset into distinct and non-overlapping regions (terminal nodes) through different partitioning criteria. In current research, the ODT with Oblique Classifier 1 (OC1) philosophy is constructed, which is generally recommended in previous studies (Murthy *et al*. 1996). By integrating the generated ODTs, the ORF model could be developed accordingly, with predictions obtained through incorporating the results of each ODT using certain ensemble methods.

2.2 Artificial neural network (ANN)

A typical ANN model is generally composed of three types of layers (i.e., input layer, hidden layer(s), and output layer), as well as the parameter weights (**W**) that connecting two adjacent layers. When using ANN to predict the responses (outputs), nonlinear functional relations are established between input and output variables, which is accomplished by determining optimal values of **W** through training process. Note that according to previous studies (Ferrario *et al*. 2017, Mangalathu *et al*. 2018), ANN models with single hidden layer could provide results with sufficient accuracy in the field of civil engineering; therefore, only one hidden layer is employed in the ANN models for the following analysis.

2.3 The ensemble ORF-ANN model

The general construction of the ORF-ANN model proposed in current research is schematically presented in Fig. 1. Note that the ORF and ANN procedures could be replaced by any other ones that possess similar function and able to complete 'classification-regression' tasks. As shown in this figure, the original dataset is first classified with the ORF algorithm, followed by the regression process completed by the ANN. The dataset for the i-th ODT (D_i in

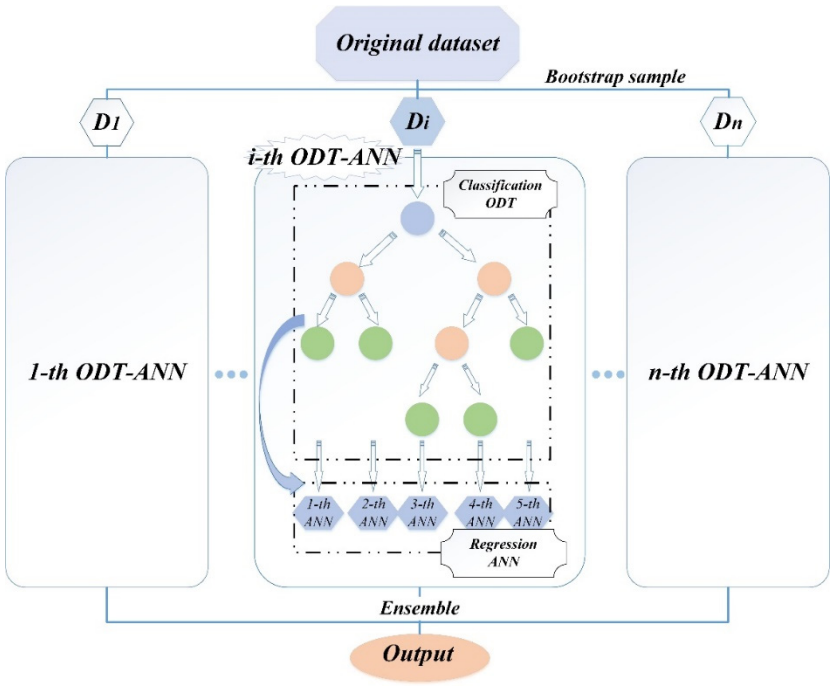

Fig. 1 Schematic construction of ORF-ANN model

Fig. 1) is developed by conducting bootstrap sampling in the original one. Then D_i is partitioned into two (or more) distinct and non-overlapping subsets through oblique splits and pre-determined partition criterion, which is repeated till all of the data in D_i are classified into terminal nodes. For each of the subsets developed in D_i, ANN model is constructed accordingly, leading to the various ODT-ANN. Finally, the ORF-ANN model could be developed by incorporating each ODT-ANN through prescribed ensemble method.

Note that the partitioning criteria such as the minimum sum of variance (regression tasks, named as R-criterion) or impurity measure (classification tasks, named as C-criteria) are generally implemented in previous literatures. In current study, the R-criterion is first utilized to develop the ORF-ANN model in the following illustration example, and the efficiency of other criteria (e.g., C-criterion) will be presented and discussed in the discussion section.

3. Framework for estimating structural seismic responses with ensemble (ORF-ANN) ML model

Based on the description of the ensemble (ORF-ANN) ML model in previous section, a framework is presented to rapidly predict the structural seismic responses.

The flowchart is plotted in Fig. 2, in which the ORF and ANN could be replaced by any proper algorithms. The

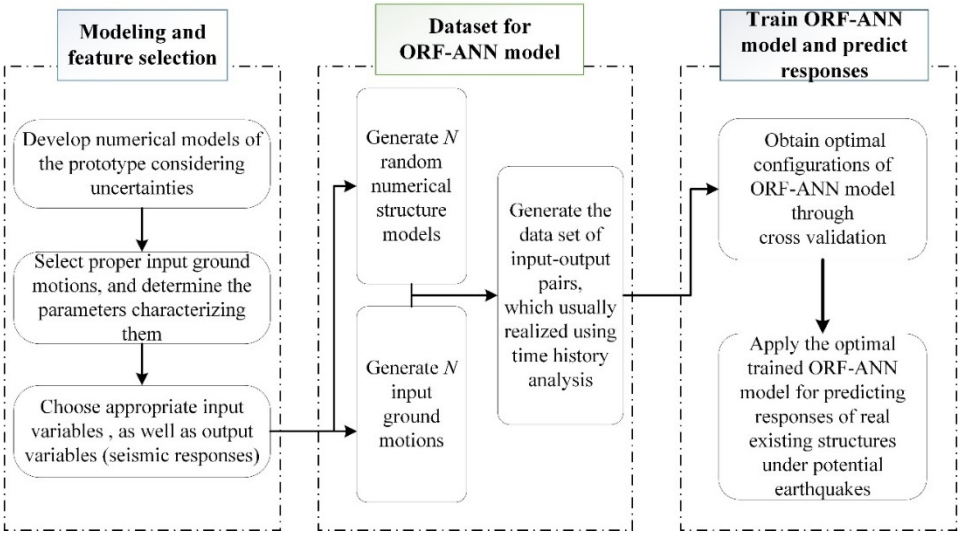

Fig. 2 The flowchart of the proposed framework

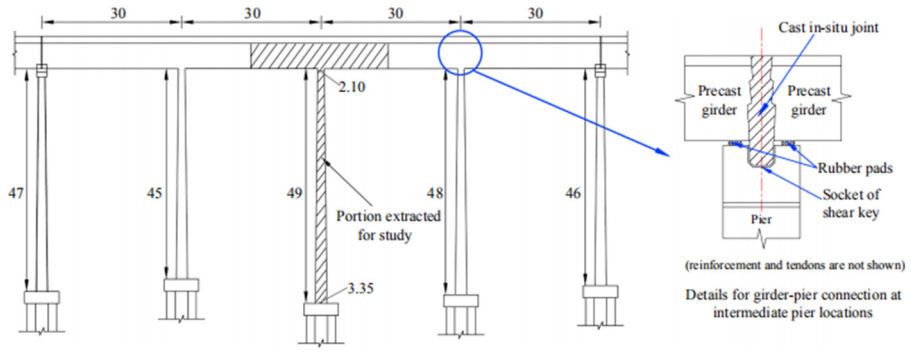

(a) Elevation of the tall pier bridge (Unit: m)

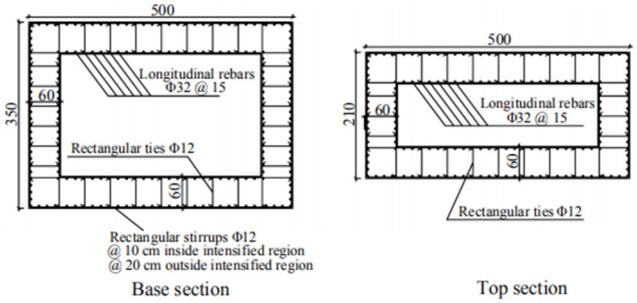

(b) Cross section of the pier column (Unit: mm for steel diameters; cm for others)

Fig 3 The prototype bridge (Chen *et al*. 2018a)

detailed steps as following:

Step 1: Develop sufficient amounts of numerical models of structure prototypes with methods such as Latin Hypercube sampling, considering uncertainties from different sources. These uncertainties will be used as parts of input variables in developing ORF-ANN models.

Step 2: Generate input excitations and randomly pair them with the numerical models developed in last step. Note that the intensity measures (IMs) characterizing ground motions should be appropriately selected and will be employed as input variables for the ORF-ANN model.

Step 3: Compute the engineering demand parameters (EDPs) through conducting NLTHA for bridge-excitation pairs. Then, the input variables selected in previous steps and corresponding EDPs are employed as input-output pairs to develop the ORF-ANN model.

Step 4: Determine the optimal configuration of ORF-ANN model with cross validation and train the model through properly. Here in this study, the *k*-fold validation procedure is employed in the following analysis, as shown in the flow chart (Fig. 2). Note that since the EDPs and IMs usually yield linear relation in logarithmic space according previous literature (Cornell *et al*. 2002), all of the EDPs and IMs are thus transformed into natural logarithmic space for better presentation in the following sections.

Step 5: Implement the trained ORF-ANN model to evaluate seismic responses of structures subjected to potential earthquake excitations. Since only the input variables (parameters characterizing structures and input motions) are required, the time efficiency could be drastically improved compared with NLTHA in this prediction task.

Note that once the proposed ORF-ANN model is properly developed, it could be used to estimate the seismic responses of a whole class of structures without re-training, which avoids the NLTHA and significantly increases time efficiency. Therefore, this framework is believed especially favored in evaluating seismic performance/post-earthquake resilience of a region and/or highway networks containing enormous structures, in which conducting NLTHA for each one is extremely computational demanding and might delay the rescue operations.

4. Illustrative examples

In current work, tall pier bridges are selected as prototype to illustrate the efficiency of the proposed framework using ORF-ANN to rapidly predict the seismic responses of structures. This type of bridges is employed due to the fact that their seismic performance has been demonstrated more complex than those with short-to-medium piers, caused by the considerable influence of distributed masses and higher-order vibration modes of pier columns (Li *et al*. 2005, Chen *et al*. 2017, Chen and Li 2020). Additionally, since these tall pier bridges usually function as key components in local transportation networks, quick assessment of their seismic responses and post-earthquake functionality is of great significance.

4.1 Analysis model description

4.1.1 The prototype bridge

A typical bridge with tall piers located in southwest China, as shown in Fig. 3, is considered herein as the

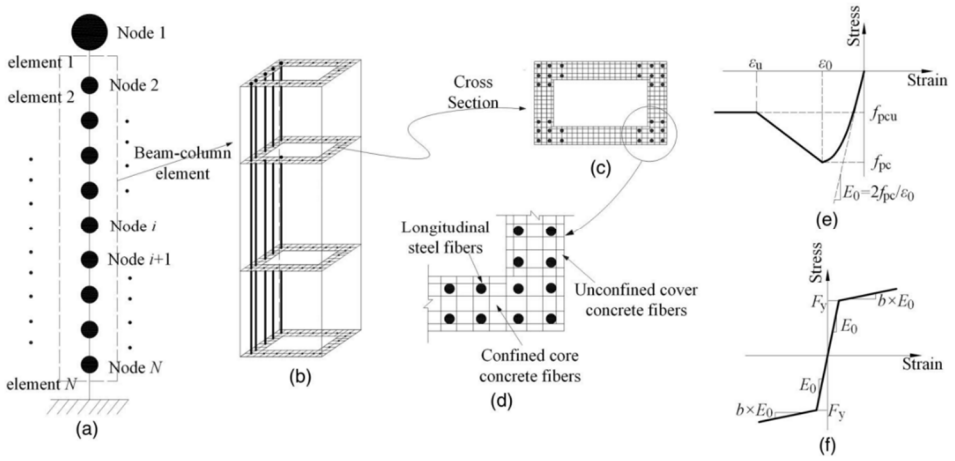

Fig. 4 Fiber elements of pier columns: (a) pier columns; (b) fiber element; (c) fiber section; (d) fiber discretion; (e) constitutive relationship for concrete; and (f) constitutive relationship for steel.

illustrated example, which was adopted in previous shake table tests (Chen *et al*. 2018a).

The superstructure is composed of four-span continuous box girder and integrated with piers by cast-in-place joints. The box girders are with uniform cross section having the width of 7.45 m and height of 3.3 m, and each span (30 m) of the box girders weights approximately 700 t. For each pier column, variable hollow sections are applied, with external dimensions ranging from 3.35 m × 5.0 m (pier base) to 2.1 m × 5.0 m (pier top) and wall thickness of 0.6 m (shown in Fig. 3(b)). At the pier base, each pier is supported by a pier cap sitting on four cast-in-place piles.

4.1.2 Finite element analysis model

According to previous shake table tests, the prototype bridge employed in current study was represented by a single mass-column system to estimate the seismic performance of the piers, as shown in Fig. 4. This simplified model was demonstrated able to reconstruct the dynamic responses during shake table tests and capture the main properties of the prototype (Chen *et al*. 2020).

The distributed masses of pier were lumped at the nodes of the column elements, while the tributary mass from two-adjacent half span of superstructure was concentrated on the pier top (Node 1). The RC pier was simulated by force-based fiber beam-column elements, which could effectively incorporate the potential nonlinear behavior during earthquake events (Taucer *et al*. 1991). The cross sections of the force-based fiber elements were composed of concrete and steel fibers (Figs. 4(c)-(d)), while the concrete fibers could be further divided into the core (confined) and cover (unconfined) fibers. According to Kent-Scott-Park material law (Scott *et al*. 1982), the constitutive relationship of the concrete material was calculated (Fig. 4(e)); and the compressive strength for cover and core fibers was 26.8 MPa and 28.5 MPa, respectively. For the steel fibers, a uniaxial bilinear relationship was introduced in current study (Guirguis and Mehanny 2013), considering kinematic hardening and optional isotropic hardening. This stress-strain relationship of steel (Fig. 4(f)) was partitioned into a linear elastic stage (E_0 = 200 GPa) with yield stress up to 400 MPa and post-yield region with strain hardening (b = 0.02).

Note that the bilinear model could not incorporate the potential damage of rebar buckling, fatigue and rupture, which are shown not that significant for structures with moderate damage (Ding *et al*. 2021), as tall piers usually undergo during earthquake events (Chen *et al*. 2018a).

4.1.3 Uncertainties

Table 1 presents different sources of uncertainties for the employed tall pier bridge, including associated probability distribution, upper and lower limit, as well as the mean values and standard deviation. Note that due to the lack of statistics about tall pier bridges in southwest China, the uncertainties of these random variables are determined by referring to previous studies (Mangalathu *et al*. 2018, 2019). Based on the data in this table, sufficient tall pier bridge samples could be randomly generated through Latin Hypercube Sampling (LHS) and applied for the following analysis.

4.2 Ground excitations and intensity measures

To evaluate the efficiency of the proposed framework and ORF-ANN model under different scenarios, two types of excitations are considered herein: filtered white noise (FWN) and artificial seismic motions (ASM). Parameters determining each type of ground excitations are properly selected, and sufficient amounts of different types of excitations will be generated. Note that these excitations will only be considered in longitudinal direction in the following analysis procedure, since the main objective of current work is to validate the efficiency of the proposed machine learning framework, rather than investigate the seismic behavior of bridge systems.

4.2.1 Filtered white noise (FWN)

FWN is widely used to simulate earthquake excitations in estimating seismic performance of structures (Aguirre and Montejo 2014, Airouche *et al*. 2014, Li *et al*. 2021). Referring to previous study, the stationary Kanai-Tajimi

Table 1 Random variables considered in current study

Random Variables	Type	Mean	Deviation	Lower Limit	Upper Limit
Superstructure					
Span length, L (m)	N*	30.0	5.0	22.0	38.0
Equivalent height of girders, h (m)	N	3.0	0.5	2.2	3.8
Width of the deck, d (m)	N	7.5	1.25	5.5	8.5
Wall thickness of girders, t_d (m)	N	0.45	0.075	0.33	0.57
Pier columns					
Pier height, H (m)	LN	50.0	5.0	43.0	58.0
Width of side wall, b (m)	LN	5.0	0.5	4.3	5.3
Width of front wall at pier base, a (m)	LN	3.5	0.35	3.01	3.99
Width of front wall at pier top, a_t (m)	LN	2.1	0.21	1.806	2.394
Wall thickness of the column, t_c (m)	LN	0.6	0.06	0.684	0.516
Other parameters					
Damping ratio, ξ	N	0.045	0.0125	0.02	0.07
Mass factor, m_f	U	1.05	0.06	0.95	1.15

*N: normal; LN: lognormal; U: uniform

(KT) model (Kanai 1957, Xu *et al*. 2017) is adopted in current research, which can be expressed as

$$\begin{aligned} \ddot{z}_g + 2\zeta_g\omega_g\dot{z}_g + \omega_g^2 z_g &= w(t) \\ a_g &= \omega_g^2 z_g + 2\zeta_g\omega_g\dot{z}_g \end{aligned} \quad (1)$$

where z_g is the filtered response; ω_g and ζ_g are the natural frequency and damping ratio of the generated motions, respectively, which are calculated according to the KT spectrum and local site conditions; $w(t)$ represents the scalar stationary white noise process, with zero-mean and constant two-sided power spectra density (PSD) of S_0; a_g denotes the absolute ground acceleration.

Following the work of Lai (1982), the mean values of ω_g and ζ_g are 20.3 rad/s and 8.97 rad/s, respectively; while the corresponding standard deviations are 0.32 and 0.13, respectively. To simulate various hazard level of earthquake excitations, the PGA of earthquakes ranging from 0.01g ~ 1.5g are adopted herein by referring to Xu *et al*. (2018). Since the root mean square (RMS) value of ground motion could be estimated to be 1/3 ~ 1/4 of PGA (Boggs 1997), the range of PSD for FWN is then corresponding to 9.71×10^{-6} ~ 0.219 computed by Eq. (2).

$$S(\omega) = \frac{\omega_g^4 + 4\zeta_g^2\omega_g^2\omega^2}{(\omega_g^2 - \omega^2)^2 + 4\zeta_g^2\omega_g^2\omega^2} S_0 \quad (2)$$

where the $S(\omega)$ and ω are power spectral density function and frequency, respectively.

4.2.2 Artificial seismic motions (ASM)

Due to the lack of recorded seismic motions for certain engineering sites, ASMs are commonly employed in estimating the seismic responses of structures in practice (Chen *et al*. 2019). In current study, the ASMs are simulated according to target design response spectra, based on the periodic function proposed by Gasparini and Vanmarck (1976)

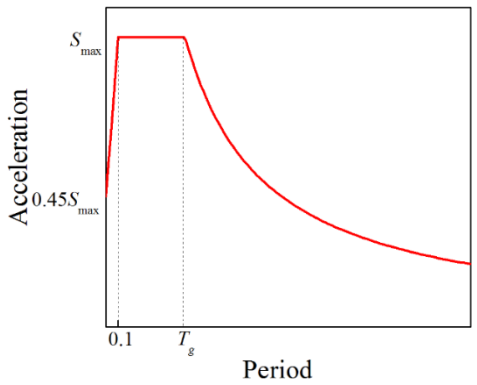

Fig. 5 Sample acceleration spectrum in Chinese specification

$$a_g = E(t)\sum_{i=1}^{N} A_i \sin(\omega_i t + \varphi_i) \quad (3)$$

where a_g denotes the time history of ground acceleration; $E(t)$ means the envelope function minimizing the errors between ASMs and actual seismic motions records; N is total number of component waves; $A(i)$ is the amplitude of the i-th component wave, determined by power spectral density function; $\omega(i)$ and ϕ_i are the natural frequency and phase angle of the i-th component wave, respectively.

The design response spectrum in Chinese code (JTG/T B02-01-2008 2008) is determined by Eqs. (4)-(5) and shown in Fig. 5. Similar to FWNs, ASMs are generated with PGA ranging from 0.14 g ~ 0.62 g to consider different hazard level of ground motions, which represents the earthquake magnitudes range from frequent to high-intensity.

Table 2 The parameters characterizing ground motions

Parameters	Name	Definition
EPV	Effective peak vel.	S_v (T = 1.0 s)/2.5
I_a	Arias intensity	$(\pi/2g)\int_0^{T_{tot}} a^2(t)d(t)$*, $a(t)$ is acc. time history
SED	Specific energy density	$\int_0^{T_{tot}} v^2(t)d(t)$, $v(t)$ is vel. time history
CAV	Cumulative absolute vel.	$\int_0^{T_{tot}} \lvert a(t)\rvert d(t)$
PGV	Peak ground vel.	Max $\lvert v(t)\rvert$
$S_a(1.0)$	Spectral acc. at 1.0s	S_a (T = 1.0 s)
$S_{v,max}/S_v(T_1)$	Ratio of maximum spectral vel. and spectral vel. at $\boldsymbol{T_1}$*	/
$S_{v,max}/S_v(T_2)$	Ratio of maximum spectral vel. and spectral vel. at $\boldsymbol{T_2}$	/
$S_{d,max}/S_d(T_1)$	Ratio of maximum spectral vel. and spectral vel. at $\boldsymbol{T_1}$	/
$S_{d,max}/S_d(T_2)$	Ratio of maximum spectral vel. and spectral vel. at $\boldsymbol{T_2}$	/
S_0	Power spectra density of FWN	/

*T_{tot} : total duration of excitation; T_1 and T_2 : fundamental and second mode period, respectively

$$S = \begin{cases} S_{\max}(5.5T + 0.45) & T < 0.1s \\ S_{max} & 0.1s \le T \le T_g \\ Sg_{max} & T > T_g \end{cases} \quad (4)$$

$$S_{\max} = 2.25 C_i C_s C_d A \quad (5)$$

where the S and $S_{\max}$ are the design and maximum value of acceleration spectrum, respectively; T is the structural period, and T_g denotes the characteristic period of engineering site; A is the design PGA; C_i, C_s, and C_d represent the coefficients corresponding to the structural significance, site category and structural damping, respectively.

4.2.3 Selection of intensity measures characterizing ground motions

The intensity measures (IMs) characterizing ground motions should be appropriately selected and employed as input variables for ML models. Table 2 show the IMs utilized for following analysis, in which such parameters as effective peak velocity (*EPV*), Arias intensity (I_a) and specific energy density (*SED*) are incorporated, since they could well recognize the features of excitations. On the other hand, to consider the interaction between excitations and structures, as well as the effects of maximum spectral values, ratios between maximum spectral velocity (displacement) and spectral velocity (displacement) at fundamental period are also considered in this table.

Since the seismic performance of tall pier bridges is significantly affected by higher-order modes, especially the second one (Chen *et al*. 2018b), ratios between maximum spectral velocity (displacement) and spectral velocity (displacement) at second mode period are employed as input as well. All of above parameters are applied to characterize both two types of excitations, while power spectra density (S_0) is adopted as an additional one for FWN.

4.3 Generation of dataset

The dataset composed of input-output pairs is generated in this sub-section, which is employed to train the ML models in following steps. Besides those listed in Table 2, the pier height (H) is adopted as one of input variables for ML models as well, since it significantly affects the performance of tall piers (Chen *et al*. 2018b). Section curvature ductility is employed as the output variable in current study, since it is the most widely accepted damage measure for tall pier bridges (Chen 2020), which is expressed as

$$\mu_\varphi = \frac{\varphi}{\varphi_y} \quad (6)$$

For each of the excitation (FWN and ASM), the dataset for training ML models is composed of 500 input-output pairs, which are obtained through conducting NLTHA for 500 bridge mode randomly paired with motions.

4.4 Optimal configurations of various ML models

4.4.1 Determination of optimal configuration

Based on the input-output pairs generated in last section, the optimal configurations of the ORF-ANN model are determined in this sub-section. Note that the models using single learning algorithms (i.e., ANN and ORF) are also developed, to better illustrate the performance of the ORF-ANN model through comparative study. By referring to previous literature (Mitchell 2014), a k-fold (k = 5) cross validation is adopted herein to obtain robust test results for the ML models with different configurations and thus determine the optimal one.

Root Mean Squared Error (RMSE) is employed to evaluate the performance of ML models, which is commonly used and expressed as (Mangalathu and Jeon 2019)

$$RMSE = \sqrt{\frac{\sum_{i=1}^{n}(\hat{Y}_i - Y_i)^2}{n}} \quad (7)$$

where n denotes the total amounts of data to be predicted; $\hat{Y}_i$ and Y_i are the seismic responses obtained from ML models and NLTHA, respectively.

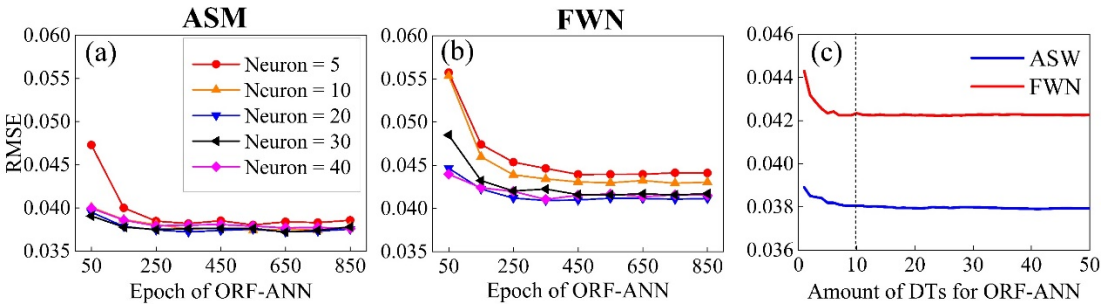

Fig. 6 Performance of ORF-ANN model with different configurations: epochs for (a) ASM & (b) FWN; (c) the amount of DTs for both ASM and FWN

As mentioned previously (Ferrario *et al*. 2017, Oh *et al*. 2020), a single hidden layer in ANN is capable of providing reliable results and adopted in current study. To find out the optimal configuration, the number of training epochs, neurons and DTs for the ORF-ANN model are originally assigned between 50 ~ 850, 5 ~ 40 and 1 ~ 50, respectively.

Fig. 6 shows the performance of ORF-ANN model with different parameters, in which the terms of ASM and FWN denote artificial seismic motion and filtered white noise, respectively. This figure illustrates that the RMSE value of ORF-ANN model first reduces with training epochs, but then remains roughly unchanged when excessive epochs are employed. Taking the ASM case with 5 neurons as an illustration (Fig. 6(a)), the RMSE is reduced by 19% with epochs increasing from 50 to 450, while remains approximately constant when epochs further increase from 450 to 850.

On the other hand, the RMSE value is affected by the amount of neurons as well, especially when lower training epochs are employed. For instance, the RMSE reduces about 17% (Fig. 6(a)) with the neuron numbers increase 5 to 40 when 50 training epochs are adopted. However, while adequate epochs are applied (e.g., 450 epochs), only a reduction around 1.5% is acquired when the neuron numbers increase from 5 to 40. This phenomenon indicates that the performance of ORF-ANN in current research is mainly dominated by the training epochs, while the effect of neuron number is not that significant. Additionally, Fig. 6(c) presents the influence of the number of DTs under both the excitations, which is observed similar to that of epochs; i.e., RMSE first decreases with the increase of DTs, and then remains unchanged when sufficient DTs are employed (10 herein).

Examination of Fig. 6 also reveals that the performance of ORF-ANN model can be significantly affected by the types of input motions. The minimized RMSE for ASM is observed around 10% lower than that of FWN. This discrepancy might be attributed to the fact that FWN is a stochastic process containing complex frequency components, and the inherent characteristics of such excitation could hardly be well recognized by limited parameters.

Based on these above analysis, Table 3 lists the optimal parameters (i.e., numbers of neurons, epochs and DTs) of the ORF-ANN model used for the following analysis, in which the corresponding parameters for ANN and ORF models are presented as well for comparison. The process of determining the optimal configurations for these single ML algorithms (i.e., ANN and ORF) is similar to that of ORF-ANN model and not shown in detailed herein for simplicity.

Table 3 Optimal configurations for various ML techniques

ML models	Neuron	Epoch	Decision tree
ORF-ANN	20	450	10
ANN	20	450	--
ORF	--	--	30

4.4.2 Performance of ML models with optimal configurations

Test subset, which is composed of 30% of dataset that are not employed for the training process, is generally employed to demonstrate the performance of ML models (Basheer and Hajmeer 2000) and examine whether overfitting (Chen *et al*. 2015, Mangalathu *et al*. 2019) exists in the developed models. That is, the ML model is believed to be efficient and have generalization capacity for newly scenarios if this model performs well on the test subset. To evaluate the performance of the optimal ORF-ANN model developed previously, the test process is conducted herein on the test subset (150 input-output pairs in total).

Fig. 7 shows the performance of ORF-ANN on both the training subset and test subset under two types of excitations, in which μ_ϕ predicted by ORF-ANN model, and 'actual' responses obtained from NLTHA are plotted into 'prediction-target' space. The corresponding fit curves and RMSE values are also presented in this figure for illustration. From Fig. 7, the predicted seismic responses on both training and test sets are observed distributing around the diagonal line, and the corresponding fit curves are roughly consistent with the line as well. This tendency indicates that the ORF-ANN obtained from previous sub-section is properly trained and performs well on the newly scenarios (test set).

Additionally, the parameters (i.e., intercept and slope) of the fit curves for test subset coincide with those of training subset under both input motions. While the RMSE values of these two subsets yield acceptable discrepancies as well; e.g., in Fig. 7(a), the RMSE value of test subset (0.037) on ASM is 5.7% higher than that of training subset (0.035).

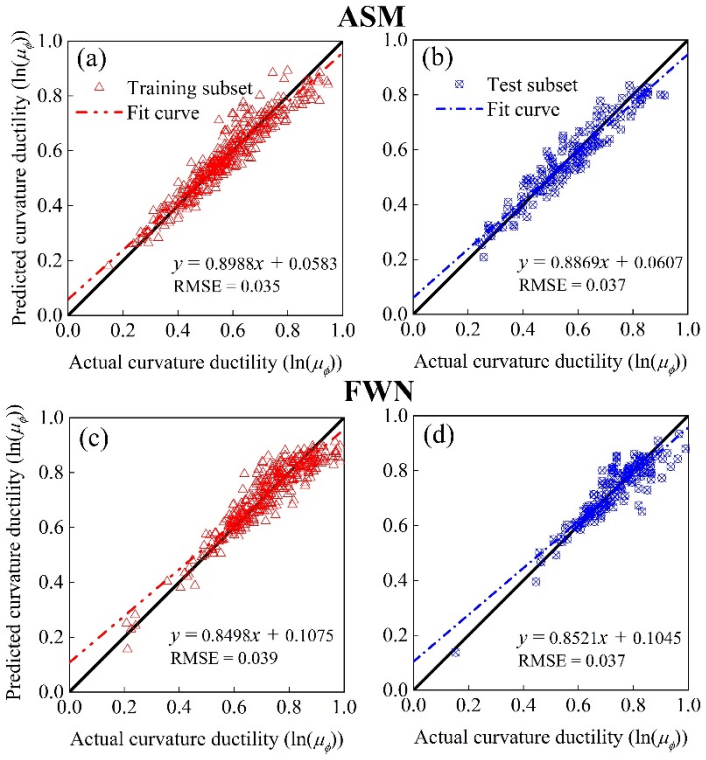

Fig. 7 Comparison between the performance of ORF-ANN on training subset and test subset

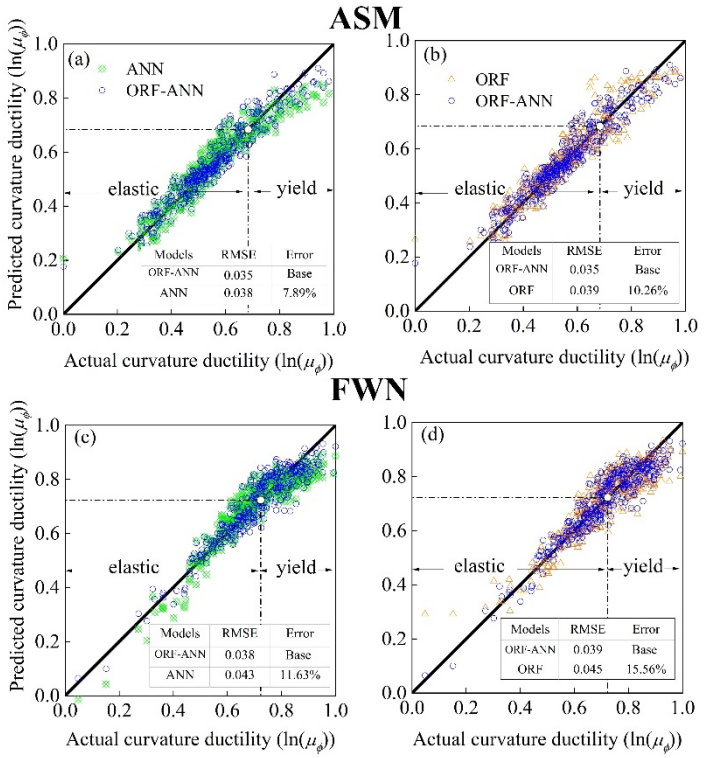

Fig. 8 400 predicted and actual results randomly selected from 1500 prediction scenarios

These phenomena again demonstrate the above conclusion, revealing that the ORF-ANN model is properly constructed without overfitting problem, and this model is capable of predicting seismic performance with considerable generalization capacity. Note that through comparing the performance of the developed single learner (i.e., ORF and ANN) on training and test subset, the results show that these two models are properly trained without overfitting as

well. The corresponding results will not be presented and discussed in detail herein to avoid redundancy.

4.5 Application of developed ML models

In this section, the properly developed ML models (ORF-ANN, ORF and ANN) will be applied to predict the seismic responses of tall pier bridges, and their efficiency will be further assessed and discussed in detailed.

To achieve this purpose, 1500 bridge-excitation scenarios (three times of the training set) are newly generated and analyzed, in which the tall pier bridges are with various design parameters (as presented in Table 2) and randomly subjected to each type of excitations. The seismic responses predicted by the proposed ORF-ANN are then compared with the results obtained from NLTHA, as well as those estimated by other ML models (i.e., ANN and ORF).

4.5.1 Overview of the predicted results

Fig. 8 plots the curvature ductility predicted by different ML techniques, as well as the 'actual' responses obtained from NLTHA in the 'prediction-target' space, while the RMSE values of each technique are also computed and presented. To provide a clearer illustration, only 400 subsets randomly selected from the totally 1500 prediction scenarios are presented in this figure, which could generally show the tendency. Note that the results are transformed into log-log space, and presented with normalized format as

$$X' = \frac{X - X_{\min}}{X_{\max} - X_{\min}} \tag{8}$$

where the X' is the normalized seismic response; $X_{\max}$ and $X_{\min}$ are the maximum and minimum seismic response, respectively; X is response of a certain realization to be normalized. The results could be then scaled into the range of 0 ~ 1.

This figure shows that all of these three ML models could be used to predict the curvature ductility of tall pier columns, since the results are generally distributed around the diagonal line in the 'prediction-target' space. While the proposed ORF-ANN model is observed with best performance for both excitations, due to the fact that this model leads to predictions closer to the diagonal line, especially when the pier columns yield under strong excitations. This feature of the proposed ORF-ANN model is of great significance in engineering practice, since nonlinear (yielding) seismic responses denote structural damage, which could deteriorate the functionality of bridges and delay the rescue operations.

On the other hand, the comparisons of RMSE values presented in Fig. 8 verify again that the proposed ORF-ANN model is more efficient than the other two single learners. Under ASM motions, the RMSE values of ORF-ANN model is 0.035, which is 7.89% and 10.26% lower than that of ANN (0.038) and ORF (0.039) model, respectively. While for FWN motions, the reductions of RMSE value are 11.63% and 15.56%, respectively, compared with ANN and ORF model. That means, the ORF-ANN model generally yields lower errors compared with both the ANN and ORF techniques when predicting the seismic responses of tall pier bridges.

4.5.1 Gaussian (*normal*) fit results

To further investigate the efficiency of the proposed model, the statistical results of the seismic responses predicted by the ORF-ANN model are calculated and compared with those obtained by NLTHA and other two single learning techniques in this sub-section. Since the structural EDPs are generally recognized and assumed to follow lognormal distribution (Padgett and Desroches 2008), the Gaussian (normal) fit process is conducted for the results obtained from NLTHA and various ML models in logarithmic space. The corresponding statistics (i.e., mean value (μ) and standard deviation (σ)) of the Gaussian fit curves for various cases could thus be computed and completely represent the characteristics of normal distribution.

Fig. 9 presents the distribution histograms, probability density functions (PDF) as well as cumulative distribution functions (CDF) obtained by different ML models and NLTHA for both the two excitations. The threshold of the linear-elastic and yield region is plotted in this figure as well. Note that in the case of FWN, the normalized responses are distributed between 0 ~ 1, but the values of the fit curves exceeding 1 are plotted in Figs. 9(d)-(f) to better illustrate the results of the fit curves.

Figs. 9(a) and (d) plot the distribution histograms of the actual curvature ductility as well as their Gaussian fit curves for ASM and FWN motions, respectively. From these two figures, the fit curves are observed matching well with the distribution histograms in both cases, indicating that the actual seismic responses obtained by NLTHA generally follow lognormal distribution, and the application of Gaussian function is reliable in this study. Similarly, the conclusion could be observed for the seismic responses obtained by different ML models and will not be presented in detail.

Figs. 9(b) and (e) present and compare the PDFs of the Gaussian fit curves under ASM and FWN, respectively. The results reveal that the PDF estimated by ORF-ANN is more consistent with that of NLTHA than other single learning techniques, especially for FWN. As shown in Fig. 9(e), the PDF estimated by ORF-ANN matches quite well with that obtained from NLTHA especially when yielding occurs; while the PDFs estimated by ANN and ORF models tend to concentrate around the mean value of the results from NLTHA, and thus underestimate the probability of the occurrence of large responses with nonlinear performance. Moreover, Figs. 9(c) and (f) illustrate the CDFs estimated by different techniques, which also shows that the ORF-ANN model leads to better estimation of EDP distribution than other two single ML models. These phenomena coincide with the results shown in Fig. 8 and denote that the ORF-ANN model could predict the seismic responses more efficiently, especially for those exceeding yielding threshold and corresponding to damage of structures.

In addition, the performance of the single learning techniques (i.e., ANN and ORF) is affected by the types of

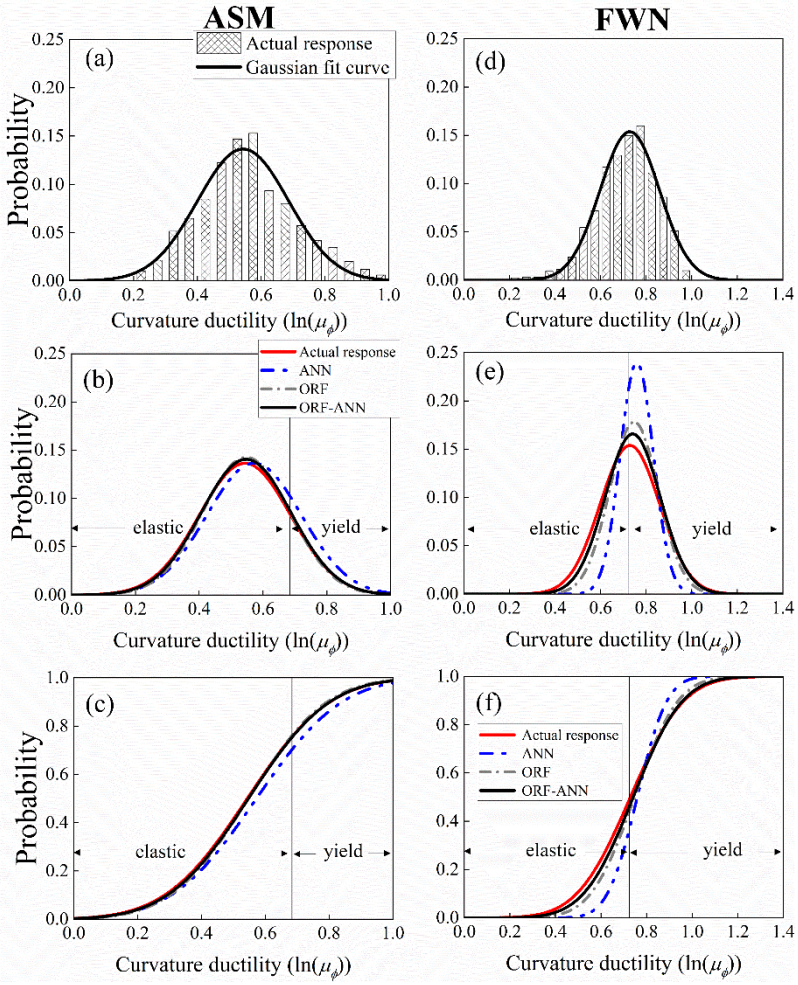

Fig. 9 Distribution histogram and PDF as well as CDF for the results of various cases: (a)-(c) ASMs; (d)-(f) FWNs

Table 4 Statistical results for the Gauss fit curves developed from various cases

Motion	Model	Mean value ($\times 10^{-2}$)		Error (%)	Deviation ($\times 10^{-2}$)		Error (%)
		Actual	Predicted	$\lvert\mu_{NL}-\mu_{ML}\rvert/\mu_{NL}$	Actual	Predicted	$\lvert\sigma_{NL}-\sigma_{ML}\rvert/\sigma_{NL}$
ASM	ORF-ANN	54.32	54.68	**0.66**	20.22	19.91	**1.53**
	ANN		57.21	5.32		20.95	3.61
	ORF		54.72	0.74		19.23	4.90
FWN	ORF-ANN	72.85	74.06	**1.66**	18.44	17.08	**7.38**
	ANN		75.87	4.15		10.26	44.36
	ORF		74.64	2.46		15.06	18.33

excitations more significantly than the ORF-ANN model. As shown in Fig. 9, ANN and ORF models perform worse for FWN scenario compared with ASM case. However, the effect of input motion types on the ORF-ANN model is not that obvious, indicating that the performance of this proposed model is more stable and robust compared with the two single learners.

Table 4 lists and compares the statistics (i.e., μ and σ) for the above different Gaussian fit curves to further illustrate the efficiency of the proposed model. The subscripts 'NL' and 'ML' denote the results obtained from NLTHA and various ML techniques, respectively.

This table shows that for both type of excitations, ORF-ANN model could provide minimized and acceptable errors in terms of both the mean value and standard deviation of the seismic responses. For instance, in the case of FWN, the error of mean value predicted by ORF-ANN is 1.66%, lower than that of ANN (4.15%) and ORF (2.46%) models. As for the standard deviation, the performance of ORF-ANN model is further improved, in which the error is 7.38%, significantly lower than that predicted by ANN (44.36%) and ORF (18.33%). This phenomenon again verifies the above conclusion that the ORF-ANN model is more efficient compared with the two single learning

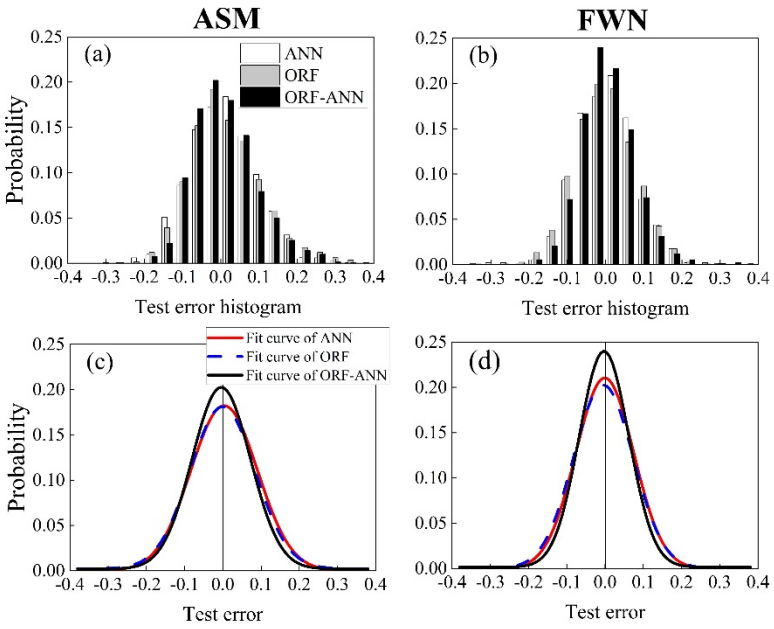

Fig. 10 Distribution of the errors for the results of ML models

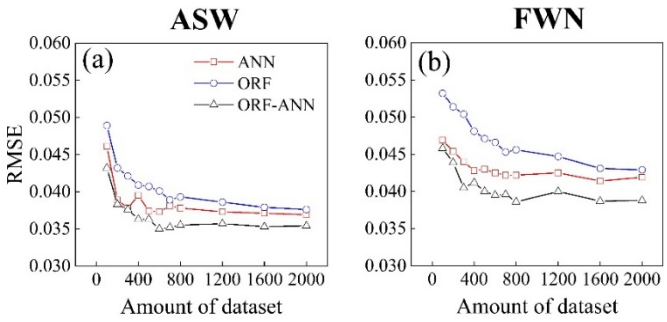

Fig. 11 The effects of various dataset for different ML models

algorithms.

4.5.2 Distribution of errors for various ML models

In this part, the errors of seismic responses obtained by various ML models are estimated and plotted through comparing with the results of NLTHA. The errors of seismic responses predicted by ML models are computed by

$$Error = \frac{|\hat{Y}_i - Y_i|}{\hat{Y}_i} \tag{9}$$

where $\hat{Y}_i$ and Y_i are the seismic responses obtained from ML models and NLTHA, respectively.

Figs. 10(a)-(b) plot the histograms of the errors for various ML models, and the Gaussian fit processes are then conducted as in previous sub-section (Figs. 9(a) and (d)), to further evaluate the performance of each ML model. The fitting results are presented in Figs. 10(c) and (d), which shows that the errors for all the ML models generally follow normal distribution; while the ORF-ANN performs better than other two ML models with higher probability around zero.

5. Discussion

To further explore the influence of other factors (e.g., scale of dataset, number of input variables, and criteria for partitioning data) on the performance of the proposed ORF-ANN model, comparative studies are conducted in this part. While the advantages and potential applications for this proposed framework and ensemble ML model is elaborated as well.

5.1 Scale of dataset

The amount of data incorporated in training set employed to develop ML models is generally recognized as a significant factor that impacts their performance. Therefore, the effects of various amounts of training data on different ML models are presented and discussed herein, in which the training sets contain data from 100 to 2000. Fig. 11 shows the corresponding results in terms of RMSE, which is obtained from trail analyses under the two types of excitations with the 5-fold cross validation procedure for each scenario.

This figure shows that the RMSE value for the proposed ORF-ANN model under both the excitations first significantly reduces with the scale of dataset, and then roughly remains constant when excessive amount of data is employed. For example, in the case of ASM, the RMSE of ORF-ANN model could reduce by 19% when training data increase from 100 to 500; however, while 2000 input-output pairs are adopted, the RMSE value generally remains unchanged and decreases around 1% compared with the that caused by dataset of 500. This tendency indicates that 500 data used for training in previous sections might be sufficient for the ORF-ANN modeling in current research, and provides acceptable results while predicting the seismic performance of tall pier bridges.

In addition, Fig. 11 also reveals that under both types of motions, the proposed ORF-ANN model could predict the seismic performance for tall pier bridges with lower errors than the single learning techniques, whatever the scale of the employed dataset is. This phenomenon coincides with the conclusion that obtained from previous section, denoting that the proposed ensemble ML model could predict the seismic performance of structures more efficiently compared with ANN and ORF model.

5.2 Various amount of input variables

The performance of ML models could be also affected by the number of the employed input variables according to previous study (Kiani *et al*. 2019). To demonstrate the efficiency of the selected parameters in current study, this part further conducts the trial analyses for the ML models that developed with more input variables.

Besides the parameters presented in Table 2, Table 5 lists the additional parameters employed as the input variables for training ML models, which are generally adopted in previous literature to characterize the features of ground motions (Wang *et al*. 2018a).

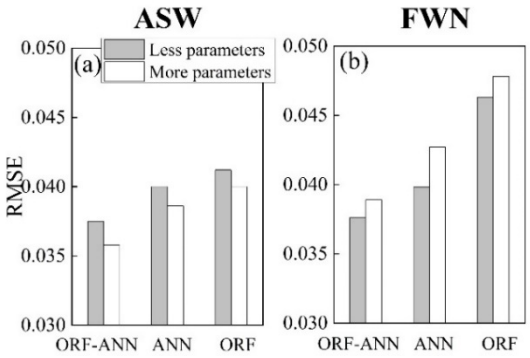

Fig. 12 The performance of various ML models on the different scenarios

Fig. 12 shows the results of the trail analyses on the performance of the different ML models developed with less (listed in Table 2) or more (with additional ones listed in Table 5) input variables. From this figure, the application of more input variables is observed only slightly decreasing the RMSE values for all of the three ML models than the less one under the ASM (Fig. 12(a)); while in the case of FWN (Fig. 12(b)), the scenario of less parameter even performs better than another when predicting seismic performance for the structures. This phenomenon reveals that the selected parameters in Table 2 might be appropriate and sufficient on the ML modeling in this research, and the application of the more parameters might not always promote the performance of ML procedure.

5.3 Partitioning criteria

As elaborated previously, the dataset is partitioned with minimum sum of variance criterion (called R-criterion) for the ORF-ANN modeling in current research, which might affect the performance of the developed model. To further

Table 5 The additional parameters selected for ML models

Parameters	Name	Definition
PGA	Peak ground acc.	Max $\|a(t)\|$, $a(t)$ is acc. time history
PGD	Peak ground disp.	Max $\|u(t)\|$, $u(t)$ is disp. time history
SD	Significant duration	$t_d = t_2 - t_1$, $t_1 = t(5\%I_a)$, $t_2 = t\ (95\%I_a)$, I_a is Arias intensity (shown in **Table 2**).
EDA	Effective design acc.	Peak acc. after filtering out frequencies beyond 9 Hz
SIR	Shaking intensity rate	$(75\%I_a - 5\%I_a)/[t(75\%I_a) - t(5\%I_a)]$
A_{rms}	Root-mean-square (RMS) of acc.	$\sqrt{\frac{1}{t_d}\int_{t_1}^{t_2} a^2(t)\,d(t)}$ t_d, t_1 and t_2 seen in ***SD***
V_{rms}	Root-mean-square (RMS) of vel.	$\sqrt{\frac{1}{t_d}\int_{t_1}^{t_2} v^2(t)\,d(t)}$
D_{rms}	Root-mean-square (RMS) of disp.	$\sqrt{\frac{1}{t_d}\int_{t_1}^{t_2} u^2(t)\,d(t)}$
EPA	Effective peak acc.	mean$[S_a(T = 0.1 \sim 0.5s)/2.5]$

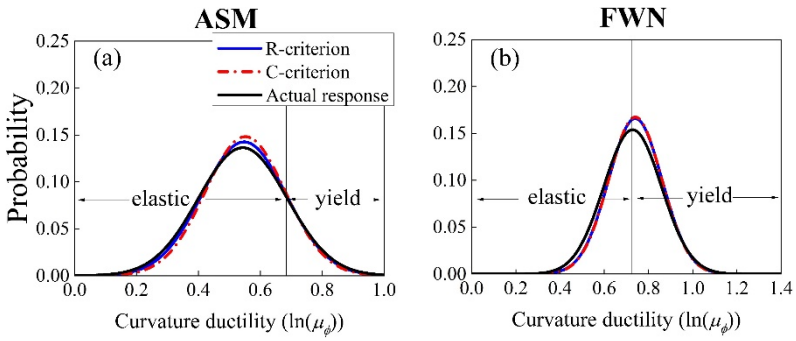

Fig. 13 Gaussian fit curves for different cases

Table 6 Statistical results for the Gaussian fit curves obtained from various cases

Wave	Criteria	RMSE	Mean value (×10^{-2})		Error (%)	Deviation (×10^{-2})		Error (%)
			Actual	Predicted	$\lvert\mu_{NL}-\mu_{ML}\rvert/\mu_{NL}$	Actual	Predicted	$\lvert\sigma_{NL}-\sigma_{ML}\rvert/\sigma_{NL}$
ASM	R-criteria	0.035	54.32	54.68	**0.66**	20.22	19.91	**1.53**
	C-criteria	0.036		55.15	1.52		18.20	10.03
FWN	R-criteria	0.038	72.85	74.06	**1.66**	18.44	17.08	**7.38**
	C-criteria	0.039		74.06	1.68		16.91	8.43

explore the effects of different partitioning criterion, the efficiency of the ORF-ANN model constructed with the minimum impurity criterion (called C-criterion) is examined in this part as well and the corresponding results are compared with that from R-criterion. Note that the Gini Index (GI) is utilized in current study as the measure of C-criterion according to Murthy *et al*. (1996). The training data are first manually labeled and categorized as 'linear-elastic' and 'yield', respectively, based on the curvature ductility obtained from NLTHA. Using the 'classification-regression' philosophy, the ORF construction among the ensemble ORF-ANN model then partitions the dataset into distinct and non-overlapped regions, followed by the regression process completed by ANN.

Fig. 13 shows the comparative results of the Gaussian fit curves for the distribution histogram obtained from the ORF-ANN models using different partitioning criteria (i.e., R- and C-criterion). From this figure, the fit curves are observed matching well with the actual responses obtained by NLTHA for both the input motion cases. In the case of ASM (Fig. 13(a)), the R-criterion model shows slightly better but comparable performance with the C-criterion one, while the fit curves of these two models almost coincide with each other for FWN (Fig. 13(b)). These phenomena indicate that the seismic performance of the tall pier bridges could be efficiently predicted by the ORF-ANN models developed base on both criteria. Note that the application of R-criterion is recommended prior to the C-criterion, since the manually labelling is avoided and the time efforts is thus minimized.

To further present the performance of these two models based on different criteria, Table 6 lists the corresponding statistical results. This table also shows that the two ORF-ANN models could both efficiently predicted the seismic performance of tall pier bridges with acceptable errors. Note that in the case of ASM, the errors of deviation on the ORF-ANN modeling with R-criterion (1.53%) is lower than the C-criterion one (10.03%). These above phenomena coincide the conclusion obtained in Fig. 13, i.e., the ORF-ANN developed with R-criterion possesses slightly better but comparable performance compared with the C-criterion one.

In addition to above two typical partitioning criteria, the proposed ORF-ANN model developed with other partitioning criteria might provide the satisfying results as well in predicting the seismic performance. In the future study, investigation concerning more partitioning criteria will be conducted, and the corresponding performance will be presented and discussed in detailed.

5.4 Advantages and potential application scenarios of the proposed framework and ensemble ML model

Since the ensemble ML model incorporates the uncertainties from excitations and different sources of structures are considered during developing procedure, it is able to predict the performance of a whole class of structures, rather than a specific one. For example, the ORF-ANN model developed in current illustration examples could be applied on bridges with tall piers (43 m to 58 m) and short-to-medium spans (22 m to 38 m), as listed in Table 1. Once properly determined through the training process, this ORF-ANN model can be directly employed estimating the seismic performance for similar bridges without any re-training.

Additionally, another significant advantage of this proposed model is that it consumes drastically less time efforts compared with NLTHA. In this paper, NLTHA procedure takes about 30 hours to obtain the seismic responses for the totally 3000 bridges subjected to two types of excitation; however, only 30 minutes are required

for the ORF-ANN model (including the parameter selection and training process, as well as the responses prediction procedure).

The time efficiency prompts this proposed model as an efficient auxiliary technique for NLTHA in engineering practice. For instance, the proposed model is especially favored during preliminary design procedure, in which the parameters of the target design bridges can be rapidly estimated with lower amounts of trail analysis compared with NLTHA. The design parameters determined by the ML-based model could be consequently used for NLTHA as references, based on which more accurate results can be obtained by developing refined FE model and conducting NLTHA if time permitted.

On the other hand, this proposed procedure and corresponding ensemble ML model could be applied to evaluate the post-earthquake state and seismic resilience of highway networks as well. Since thousands of bridge systems might be contained in regional highway networks, conducting the NLTHA for each of them with different design parameters can be prohibitively time consuming. While with the application of the proposed model, the post-earthquake damage states for these bridges could be thus estimated rapidly, and the plans of rescue operations can be proposed instantaneously, reducing the potential financial and lift loss.

6. Conclusions

This paper proposes a framework based on ensemble machine learning philosophy, to promote the efficiency of evaluating structural seismic responses. Although ORF and ANN are employed in current study, they are used for illustration and could be replaced by any other ML techniques yielding better performance. From the analytical results of illustrative example of tall pier bridges, the following conclusion could be obtained:

- The ensemble model (ORF-ANN herein) performs better than the separate single learning algorithms (i.e., ANN and ORF), in terms of both errors (represented by RMSE) and distribution patterns of predicted responses. Additionally, this ORF-ANN model is demonstrated more robust and stable than ANN and ORF when different types of input motions are considered.
- Once properly developed, the ensemble ML model could be applied to a whole class of structures without re-training. Therefore, the efficiency of structural design could be significantly improved by determining parameters rapidly and reducing the amount of trial analyses.
- When conducting analysis for enormous structures, the proposed ORF-ANN model could increase time efficiency over 95% compared with NLTHA. Consequently, this model is believed especially appropriate for evaluating the post-earthquake states and seismic resilience of a region and/or highway networks, where numerous structures might be contained. Conducting NLTHA for each structural would be prohibitively time consuming and delay rescue operations; while the proposed model could facilitate the rescue planning and reduce potential financial and life loss.
- Selecting input variables for ML models considering characteristics of structures and ground motions, as well as their interactions, could significantly improve the efficiency.
- Various partitioning criteria might be used to complete the classification task in the proposed model, while that avoid manually labeling (R-criterion) is recommended to minimize the efforts of human beings.

Future work might be conducted to further improve the efficiency of this ensemble ML model, finding out better techniques to replace ORF and ANN, as well as more appropriate criteria for classification.

Acknowledgments

The authors gratefully acknowledge the support by the National Natural Science Foundation (No. 51908348 & 51778354). The corresponding author also acknowledges the support of *Shanghai Post-doctoral Excellence Program*.

References

Aguirre, D.A. and Montejo, L.A. (2014), "Damping and frequency changes induced by increasing levels of inelastic seismic demand", *Smart Struct. Syst., Int. J.*, **14**(3), 445-468. http://doi.org/10.12989/sss.2014.14.3.445

Airouche, A., Bechtoula, H., Aknouche, H., Thoen, B.K. and Benouar, D. (2014), "Experimental identification of the six dof cgs, algeria, shaking table system", *Smart Struct. Syst., Int. J.*, **13**(1), 137-154. http://doi.org/10.12989/sss.2014.13.1.137

Alam, R., Peden, D. and Lach, J. (2020), "Wearable respiration monitoring: Interpretable inference with context and sensor biomarkers", *IEEE J. Biomed. Health Inform.*, **25**(6), 1938-1948. http://doi.org/10.1109/jbhi.2020.3035776

Basheer, I.A. and Hajmeer, M. (2000), "Artificial neural networks: Fundamentals, computing, design, and application", *J. Microbiol. Methods*, **43**(1), 3-31. http://doi.org/10.1016/S0167-7012(00)00201-3

Boggs, D. (1997), "Acceleration indexes for human comfort in tall buildings–Peak or RMS", *CTBUH Monogr.*, 1-21.

Breiman, L. (2001), "Random forests", *Mach. Learn.*, **45**(1), 5-32. http://doi.org/10.1023/a:1010933404324

Chen, X. (2020), "System fragility assessment of tall-pier bridges subjected to near-fault ground motions", *J. Bridge Eng.*, **25**(3), 04019143. http://doi.org/10.1061/(asce)be.1943-5592.0001526

Chen, X. and Li, C. (2020), "Seismic performance of tall pier bridges retrofitted with lead rubber bearings and rocking foundation", *Eng. Struct.*, **212**, 110529. http://doi.org/10.1016/j.engstruct.2020.110529

Chen, K., Gong, S., Xiang, T. and Loy, C.C. (2013), "Cumulative attribute space for age and crowd density estimation", Proceedings of 2013 IEEE Conference on Computer Vision and Pattern Recognition, Portland, OR, USA, June.

Chen, Z.H., Ni, Y.Q. and Or, S.W. (2015), "Characterization and modeling of a self-sensing mr damper under harmonic loading", *Smart Struct. Syst., Int. J.*, **15**(4), 1103-1120. http://doi.org/10.12989/sss.2015.15.4.1103

Chen, X., Li, J. and Liu, X. (2017), "Seismic performance of tall piers influenced by higher-mode effects of piers", *J. Tongji Univ.* (*Natural Science*), **45**(02), 159-166.

Chen, X., Guan, Z., Li, J. and Spencer, B.F. (2018a), "Shake table tests of tall-pier bridges to evaluate seismic performance", *J. Bridge Eng.*, **23**(9), 04018058. http://doi.org/10.1061/(asce)be.1943-5592.0001264

Chen, X., Guan, Z., Spencer, B.F. and Li, J. (2018b), "A simplified procedure for estimating nonlinear seismic demand of tall piers", *Eng. Struct.*, **174**, 778-791. http://doi.org/10.1016/j.engstruct.2018.07.102

Chen, P.-C., Hsu, S.-C., Zhong, Y.-J. and Wang, S.-J. (2019), "Real-time hybrid simulation of smart base-isolated raised floor systems for high-tech industry", *Smart Struct. Syst., Int. J.*, **23**(1), 91-106. http://doi.org10.12989/sss.2019.23.1.091

Chen, X., Xiang, N., Li, J., and Guan, Z. (2020), "Influence of near-fault pulse-like motion characteristics on seismic performance of tall pier bridges with fragility analysis", *J. Earthq. Eng.*, 1-22. http://doi.org/10.1080/13632469.2020.1751345

Chopra, A.K. and Goel, R.K. (2002), "A modal pushover analysis procedure for estimating seismic demands for buildings", *Earthq. Eng. Struct. Dyn.*, **31**(3), 561-582. http://doi.org/10.1002/eqe.144

Cornell, C.A., Jalayer, F., Hamburger, R.O. and Foutch, D.A. (2002), "Probabilistic basis for 2000 sac federal emergency management agency steel moment frame guidelines", *J. Struct. Eng.-ASCE*, **128**(4), 526-533. http://doi.org/10.1061/(asce)0733-9445(2002)128:4(526)

Das, R. and Sengur, A. (2010), "Evaluation of ensemble methods for diagnosing of valvular heart disease", *Expert Syst. Applicat.*, **37**(7), 5110-5115. http://doi.org/10.1016/j.eswa.2009.12.085

Ding, Y., Wu, D., Su, J., Li, Z.-X., Zong, L. and Feng, K. (2021), "Experimental and numerical investigations on seismic performance of RC bridge piers considering buckling and low-cycle fatigue of high-strength steel bars", *Eng. Struct.*, **227**, 111464. http://doi.org/10.1016/j.engstruct.2020.111464

Duan, Y., Chen, Q., Zhang, H., Yun, C.B., Wu, S. and Zhu, Q. (2019), "Cnn-based damage identification method of tied-arch bridge using spatial-spectral information", *Smart Struct. Syst., Int. J.*, **23**(5), 507-520. http://doi.org/10.12989/sss.2019.23.5.507

Ferrario, E., Pedroni, N., Zio, E. and Lopez-Caballero, F. (2017), "Bootstrapped artificial neural networks for the seismic analysis of structural systems", *Struct. Safety*, **67**, 70-84. http://doi.org/10.1016/j.strusafe.2017.03.003

Gasparini, D. and Vanmarcke, E. (1976), "Simulated earthquake motions compatible with prescribed response spectra", MIT Department of Civil Engineering Research Report NO. R76-4; Massachusetts Institute of Technology, Cambridge, MA, USA.

Guirguis, J. and Mehanny, S.S.F. (2013), "Evaluating code criteria for regular seismic behavior of continuous concrete box girder bridges with unequal height piers", *J. Bridge Eng.*, **18**(6), 486-498. http://doi.org/10.1061/(ASCE)BE.1943-5592.0000383

JTG/T B02-01-2008 (2008), Guidelines for seismic design of highway bridges, Chongqing communications scientific research design institute; Beijing, Ministry of Transport of the People's Republic of China.

Kanai, K. (1957), "Semi-empirical formula for the seismic characteristics of the ground", *Bull. Earthq. Res. Inst.*, **35**(2), 309-325. http://doi.org/10.3130/aijsaxx.57.1.0_281

Kiani, J., Camp, C. and Pezeshk, S. (2019), "On the application of machine learning techniques to derive seismic fragility curves", *Comput. Struct.*, **218**, 108-122. http://doi.org/10.1016/j.compstruc.2019.03.004

Lai, S.-S. (1982), "Statistical characterization of strong ground motion using power spectral density function", *Bull. Seismol. Soc. Am.*, **72**(1), 259-274. https://doi.org/10.1785/BSSA0720010259

Li, J., Song, X. and Fan, L. (2005), "Investigation for displacement ductility capacity of tall piers", *Earthq. Eng. Eng. Vib.*, **25**(1), 43-48.

Li, C., Chang, K., Cao, L. and Huang, Y. (2021), "Performance of a nonlinear hybrid base isolation system under the ground motions", *Soil Dyn. Earthq. Eng.*, **143**, 106589. https://doi.org/10.1016/j.soildyn.2021.106589

Liu, Z. and Zhang, Z. (2017), "Artificial neural network based method for seismic fragility analysis of steel frames", *KSCE J. Civil Eng.*, **22**(2), 708-717. http.//doi.org/10.1007/s12205-017-1329-8

Mangalathu, S. and Jeon, J.-S. (2019), "Stripe-based fragility analysis of multispan concrete bridge classes using machine learning techniques", *Earthq. Eng. Struct. Dyn.*, **48**(11), 1238-1255. http://doi.org/10.1002/eqe.3183

Mangalathu, S., Heo, G. and Jeon, J.-S. (2018), "Artificial neural network based multi-dimensional fragility development of skewed concrete bridge classes", *Eng. Struct.*, **162**, 166-176. http://doi.org/10.1016/j.engstruct.2018.01.053

Mangalathu, S., Hwang, S.-H., Choi, E. and Jeon, J.-S. (2019), "Rapid seismic damage evaluation of bridge portfolios using machine learning techniques", *Eng. Struct.*, **201**, 109785. http://doi.org/10.1016/j.engstruct.2019.109785

Mitchell, J. (2014), "Machine learning methods in chemoinformatics", *Wiley Interdiscipl. Rev.: Computat. Molecul. Sci.*, **4**, 468-481. http://doi.org/10.1002/wcms.1183

Murthy, S., Kasif, S. and Salzberg, S. (1996), "A system for induction of oblique decision trees", *J. Artif. Intell. Res.*, **2**, 1-32. http://doi.org/10.1613/jair.63

Oh, B.K., Glisic, B., Park, S.W. and Park, H.S. (2020), "Neural network-based seismic response prediction model for building structures using artificial earthquakes", *J. Sound Vib.*, **468**, 115109. http://doi.org/10.1016/j.jsv.2019.115109

Onat, O. and Gul, M. (2018), "Application of artificial neural networks to the prediction of out-of-plane response of infill walls subjected to shake table", *Smart Struct. Syst., Int. J.*, **21**(4), 521-535. http://doi.org/10.12989/sss.2018.21.4.521

Padgett, J. and Desroches, R. (2008), "Methodology for the development of analytical fragility curves for retrofitted bridges", *Earthq. Eng. Struct. Dyn.*, **37**, 1157-1174. http://doi.org/10.1002/eqe.801

Pang, Y., Zhou, X., He, W., Zhong, J. and Hui, O. (2021), "Uniform design–based Gaussian process regression for data-driven rapid fragility assessment of bridges", *J. Struct. Eng.*, **147**(4), 04021008. http://doi.org/10.1061/(asce)st.1943-541x.0002953

Saeidpour, A., Chorzepa, M.G., Christian, J. and Durham, S. (2018), "Parameterized fragility assessment of bridges subjected to hurricane events using metamodels and multiple environmental parameters", *J. Infrastr. Syst.*, **24**(4), 04018031. http://doi.org/10.1061/(asce)is.1943-555x.0000442

Scott, B.D., Park, R. and Priestley, M.J.N. (1982), "Stress-strain behaviour of concrete confined by overlapping hoops at low and high strain rates", *J. Am. Concrete Inst.*, **79**, 13-27.

Taucer, F., Spacone, E. and Filippou, F. (1991), "A fiber beam-column element for seismic response analysis of reinforced concrete structures", Report No. UCB/EERC-91/17; Earthquake Engineering Research Center, College of Engineering, University of California Berkekey, CA, USA.

Wang, X., Shafieezadeh, A. and Ye, A. (2018a), "Optimal intensity measures for probabilistic seismic demand modeling of extended pile-shaft-supported bridges in liquefied and laterally spreading ground", *Bull. Earthq. Eng.*, **16**(1), 229-257. http://doi.org/10.1007/s10518-017-0199-2

Wang, Z., Pedroni, N., Zentner, I. and Zio, E. (2018b), "Seismic

fragility analysis with artificial neural networks: Application to nuclear power plant equipment", *Eng*. *Struct*., **162**, 213-225. http://doi.org/10.1016/j.engstruct.2018.02.024

Wang, L., Li, J., Zhang, S., Zhang, X., Zhang, Q., Chan, M.F., Yang, R. and Sui, J. (2020), "Multi-task autoencoder based classification-regression model for patient-specific VMAT QA", *Phys*. *Medic*. *Biol*., **65**(23), 235023. http://doi.org/10.1088/1361-6560/abb31c

Xie, Y., Ebad Sichani, M., Padgett, J.E. and DesRoches, R. (2020), "The promise of implementing machine learning in earthquake engineering: A state-of-the-art review", *Earthq*. *Spectra*, **36**(4), 1769-1801. http://doi.org/10.1177/8755293020919419

Xu, J., Spencer Jr, B.F. and Lu, X. (2017), "Performance-based optimization of nonlinear structures subject to stochastic dynamic loading", *Eng*. *Struct*., **134**, 334-345. http://doi.org/10.1016/j.engstruct.2016.12.051

Xu, J., Fermandois, G.A., Spencer, B.F., Jr. and Lu, X. (2018), "Stochastic optimisation of buckling restrained braced frames under seismic loading", *Struct*. *Infrastr*. *Eng*., **14**(10), 1386-1401. http://doi.org/10.1080/15732479.2018.1443144

Zhang, L. and Suganthan, P.N. (2015a), "Oblique decision tree ensemble via multisurface proximal support vector machine", *IEEE Trans*. *Cybern*., **45**(10), 2165-2176. http://doi.org/10.1109/tcyb.2014.2366468

Zhang, L. and Suganthan, P.N. (2015b), "Oblique decision tree ensemble via multisurface proximal support vector machine", **45**(10), 2165-2176. http://doi.org/10.1109/TCYB.2014.2366468

Zhang, L. and Suganthan, P. (2017), "Benchmarking ensemble classifiers with novel co-trained kernal ridge regression and random vector functional link ensembles [research frontier]", *IEEE Computat*. *Intell*. *Magaz*., **12**, 61-72. http://doi.org/10.1109/MCI.2017.2742867

BS